

## Supporting Information

### **Defect Repair of Tin Selenide Photocathode via In-Situ Selenization: Enhanced Photoelectrochemical Performance and Environmental Stability**

Ruilun Wang<sup>a,c</sup>, Yanhong Lyu<sup>\*a,c</sup>, Shiqian Du<sup>a,c</sup>, Shiyong Zhao<sup>b</sup>, Hao Li<sup>a,c</sup>, Li Tao<sup>a,c</sup>, San Ping Jiang<sup>b</sup>, Jianyun Zheng<sup>\*a,c</sup> and Shuangyin Wang<sup>\*a,c</sup>

#### **Experimental Section**

*Materials:* Sn powder, Se powder and sulfuric acid were obtained from Shanghai Chemical Reagents, China. All of the chemicals used in this experiment were of analytical grade and used without further purification.

*Synthesis of pristine tin selenide:* SnSe thin films were deposited by facile thermal vacuum evaporation of a mixed Sn and Se powder source onto fluorine-doped tin oxide (FTO) glass substrates at a base pressure of around  $10^{-4}$  Pa. The mixed Sn powder and Se powder were prepared in a ratio of 1:1 to prepare a reagent A. Reagent A (0.1g) was placed in the evaporation boat 1. Turn on the vacuum pump and the vacuum to  $1 \times 10^{-3}$  Pa or less, opening the baffle and adjusting the evaporation current to 90 A for 10 minutes, then increasing the current to 110 A for 5 minutes and turn off the evaporation switch. The sample plate was heated to 150 °C and annealing was continued for 2 hours in vacuum. Finally, Waiting for the sample was taken out after cooling.

*Synthesis of repaired tin selenide:* A same method to above. Preparation of reagent A, forming vacuum environment, evaporation sample, annealing and cooling. Differently, a small amount of Se powder (0.002-0.016g) was added to the evaporation boat 2. When the annealing was carried out one and half hours, the Se powder of the evaporation boat 2 was evaporated. Annealing at 150 °C was continued for half hour and then cooled and obtained the sample. Comparing the different selenium (Path 2), the sample was named to P-SnSe, R-SnSe-L1, R-SnSe-L2 (R-SnSe-L), R-SnSe-M1 (R-SnSe-M), R-SnSe-M2, R-SnSe-H

corresponding the 0, 2, 6, 8, 10, 14 mg selenium during selenization, respectively (in Supporting Information).

*Materials characterizations:* The surface of semiconductor were determined by atomic force microscope (AFM, Bruker Bioscope system). To investigate the crystalline structure of samples, a Rigaku diffractometer (Rigaku Ultima IV) using Cu K $\alpha$  radiation ( $\lambda = 0.15406$  nm) was employed to performing  $2\theta$  X-ray diffraction (XRD) scans with the grazing angle of  $1^\circ$  at the scan rate of  $2^\circ \text{ min}^{-1}$ . XPS measurements were carried out with an ESCALAB 250Xi using a monochromic Al X-ray source. All binding energies were referenced to the C1s peak (284.8 eV) arising from adventitious carbon. The morphology and microstructure of samples were investigated by field emission scanning electron microscope (FESEM, Hitachi, S-4800). The composition was tested by line-scanning energy dispersive x-ray spectroscopy (EDS) attached FESEM. The Raman spectra were collected on a Raman Spectrometer (Labram-010) using 532 nm laser. Photoluminescence (PL) spectra were measured at room temperature on a fluorescence spectrophotometer (Fls-980, Edinburgh). Time-resolved PL decay spectra were measured using a fluorescence lifetime spectrometer (Fls-980). The PL lifetime of all the samples were calculated by fitting the experimental decay transient data with bi-exponential decay model. EPR spectra were taken on a JES FA-200 (JEOL) continuous-wave EPR spectrometer by applying an X band (9.2 GHz) and a sweeping magnetic field at  $0^\circ \text{C}$ . NEAXFS The optical transmittance characteristics were monitored on a UV-visible-near-IR spectrophotometer (Hitachi, UV-4100) at normal incidence from 350 to 2600 nm. The absorption coefficient relate to the transmittance  $T$  and film thickness  $d$  as following:

$$F(R) = \frac{(1-R)^2}{2R} \cong \alpha \quad (1)$$

The optical energy band gap of the sample has been estimated by using the classical relation of optical absorption

$$\alpha hv = B(hv - E_g)^m \quad (2)$$

Where B,  $E_g$  and  $h\nu$  denote as the band tailing parameter, the optical band gap and the photon energy, respectively. The value of  $m$  should be taken as 2, a characteristic value for the direct allowed transition which dominates over the optical absorption.

*Electrochemical measurements:* The electrochemical measurements were performed in a three-electrode system using an electrochemical workstation (CHI 760E). A FTO electrode was used as working electrode, Pt mesh as counter electrode and Ag/AgCl as the reference electrode were used as counter electrode and reference electrode, respectively. The Mott-Schottky plots were acquired at a frequency of 10 KHz in 0.05 M aqueous  $H_2SO_4$  solution by a CHI 760 potentiostat. The Mott-Schottky equation is shown below:

$$\frac{1}{C^2} = \frac{2(V - V_{fb} - kT/q)}{q\epsilon_s\epsilon_0 A^2 N_D} \quad (3)$$

where  $C$  is capacitance,  $q$  the charge of an electron ( $1.60 \times 10^{-19}$  C),  $\epsilon_0$  the vacuum permittivity ( $8.85 \times 10^{-14}$  F·cm<sup>-1</sup>),  $\epsilon_s$  the permittivity of tin selenium (80 F·cm<sup>-1</sup>),  $A$  the area of the sample,  $N_D$  the donor density,  $V$  the applied bias,  $V_{fb}$  the flat band voltage,  $k$  Boltzmann's constant ( $1.38 \times 10^{-23}$  J·K<sup>-1</sup>), and  $T$  the temperature (25 °C). The x-intercept of the Mott-Schottky plot was reached at the bias that needs to be applied to cause the bands to become flat.

*PEC measurement:* A three-electrode cell (that is, Si-based photocathode as the working electrode, Pt wire as the counter electrode and Ag/AgCl as the reference electrode) was implemented for PEC measurements in 0.05 M aqueous  $H_2SO_4$  by a PEC 1000 system (PerfectLight Co. Ltd.) with illumination of solar light (AM 1.5G, 100 mW·cm<sup>-2</sup>) using a solar simulator (optical fiber source, FX300). Before each measurement, the solar simulator intensity was calibrated with a reference silicon solar cell and a readout meter for the solar simulator irradiance (PerfectLight Co. Ltd., PL-MW 200). Linear-sweep voltammetry (J-V)

data without any iR compensation were collected using a CHI 630E electrochemical workstation with or without illuminating. For a typical J-V measurement, the voltage was swept linearly at a scan rate of 0.005 V·s<sup>-1</sup>. Readings for Ag/AgCl were converted to RHE using the following relationship.

$$E \text{ (RHE)} = E \text{ (Ag/AgCl)} + 0.197 \text{ V} + 0.059 \times \text{pH} \quad (4)$$

IPCE measurements were conducted in 0.05 M H<sub>2</sub>SO<sub>4</sub> aqueous solution at -0.2 V vs RHE. The solar simulator (AM 1.5 G, 100 mW cm<sup>-2</sup>) connected a monochrome filter (from 380 to 700 nm) provided monochromatic illumination. Each testing at each wavelength was the dark of 2 s and then the illumination of 2 s. The current was collected at 10 points per second. The final 10 points of each light and dark cycle were averaged. The photocurrent was equal to the light current subtracting the dark current. IPCE was calculated by the equation

$$\text{IPCE} = \left[ \frac{1240 \times (J_{\text{light}} - J_{\text{dark}})}{\lambda P_{\lambda}} \right] \times 100\% \quad (5)$$

where  $J_{\text{light}}$ ,  $J_{\text{dark}}$ ,  $\lambda$  and  $P_{\lambda}$  denote light current, dark current, certain wavelength, density of light intensity at certain wavelength, respectively.

The Faradaic efficiency (FE) were calculated by the equation:

$$FE = \frac{2 \times 96485 \times [\text{H}_2] \times V}{M_{\text{H}_2} \times Q} \quad (6)$$

where  $[\text{H}_2]$ ,  $V$ ,  $M_{\text{H}_2}$  and  $Q$  are the measured average H<sub>2</sub> concentration, the volume of gas, the molecular weight of H<sub>2</sub>, and the total charge passed through the electrode, respectively.

## Supplementary Figures

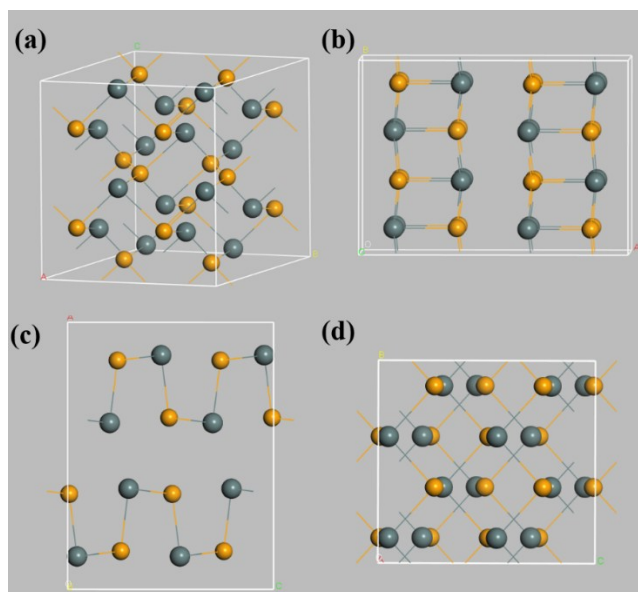


Figure S1. Simulated SnSe crystal structure: (a) simulated structure at xyz-axis: Blue, Sn atoms; yellow, Se atoms (b) structure along the z-axis (c) structure along the y-axis (d) structure along the x-axis.

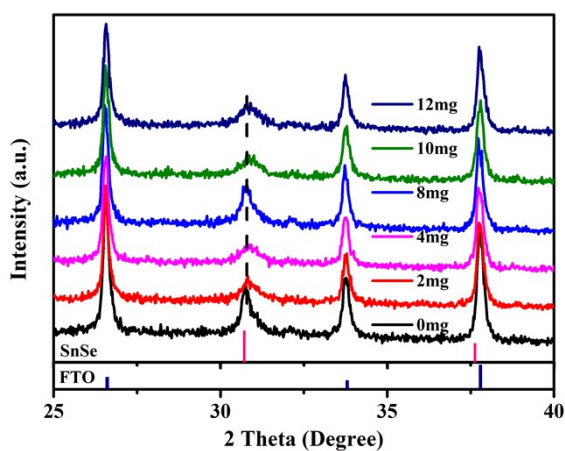


Figure S2. XRD pattern for different sample. The XRD ensure the present of SnSe. At the same time, the intensity of peak is first decrease and then returning to the same width from 0 mg to 8 mg. After excessive selenization, the intensity of peak in continue decrease. The phenomenon indicates the crystallize level for SnSe, which means transition states is existed in selenization process.

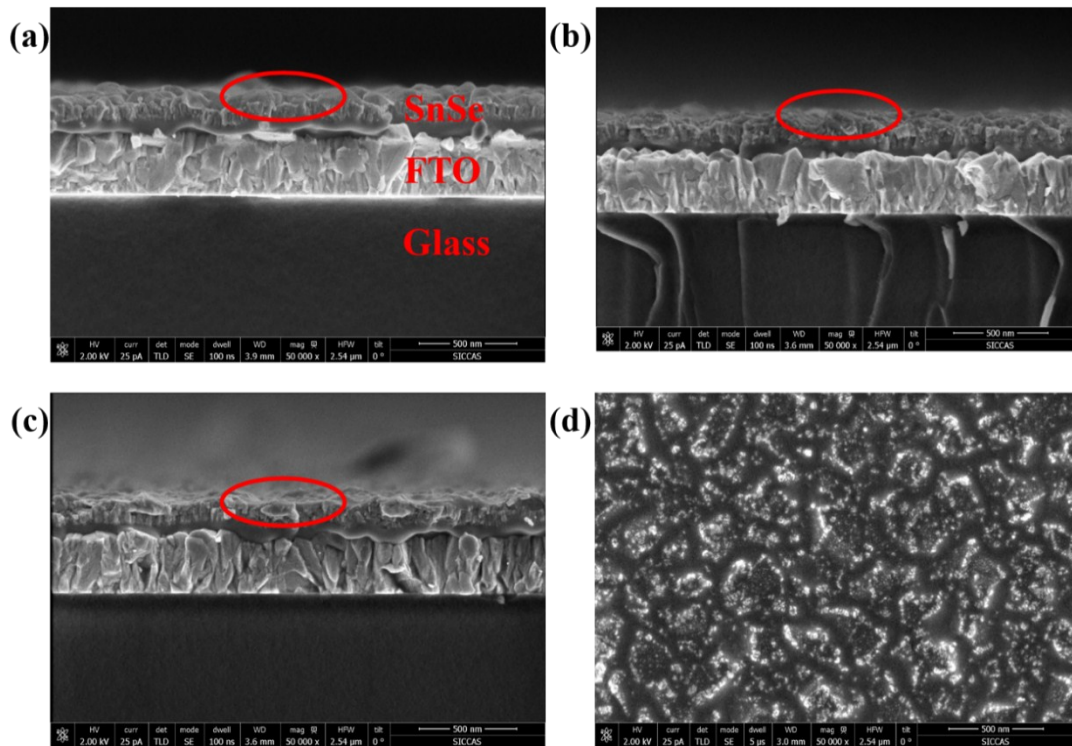


Figure S3. SEM images of (a) 0 mg (b) 4 mg (c) 8 mg (d) the surface of 8 mg

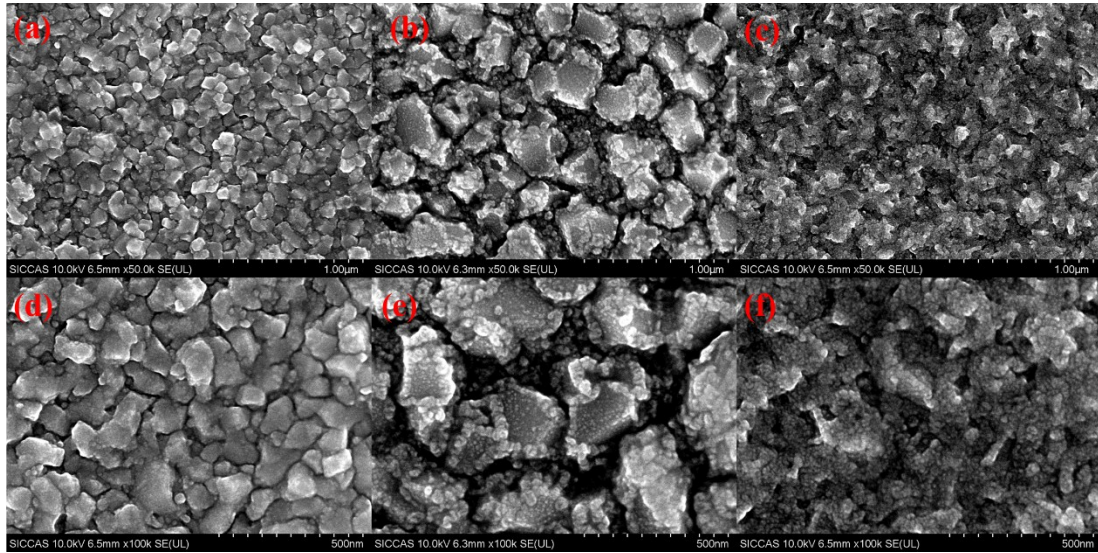


Figure S4. SEM images of the surface morphology for the samples: (a), (d) P-SnSe; (b), (e) R-SnSe-L; (c), (f) R-SnSe-H.

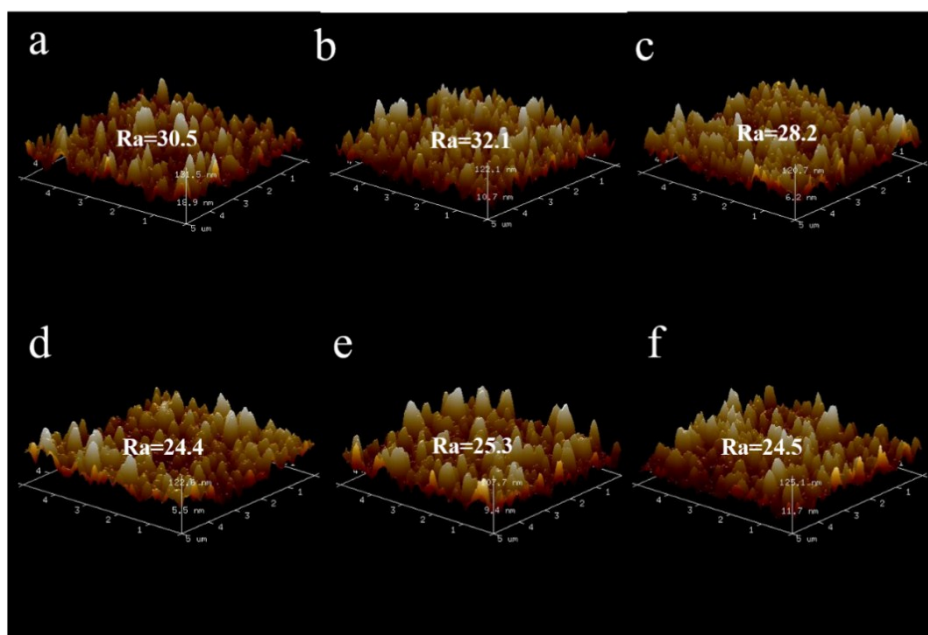


Figure S5. AFM images of (a) 0 mg (b) 2 mg (c) 6 mg (d) 8 mg (e) 10 mg (f) 14 mg

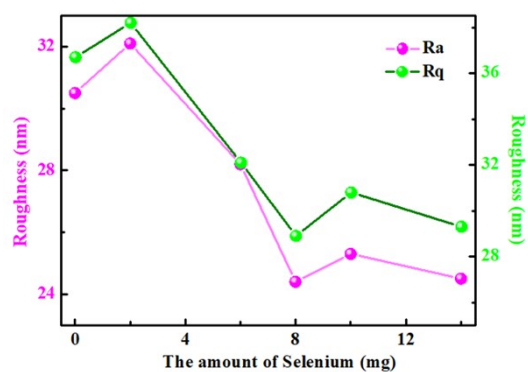


Figure S6. Tendency of roughness on surface for different selenium.

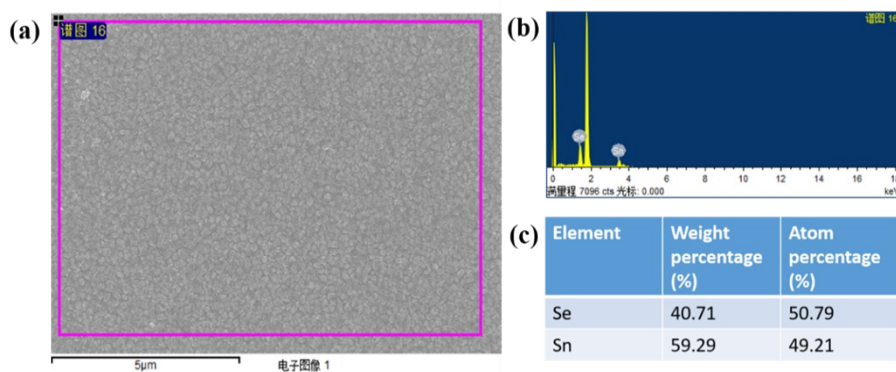


Figure S7. Sn and Se elemental ratio of 0 mg

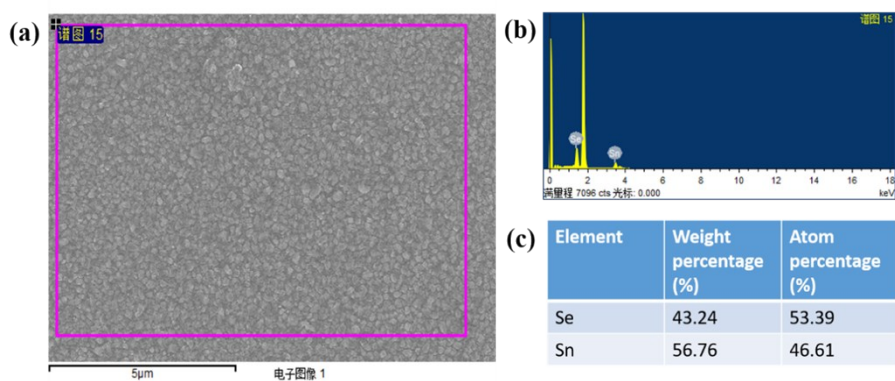


Figure S8. Sn and Se elemental ratio of 8 mg

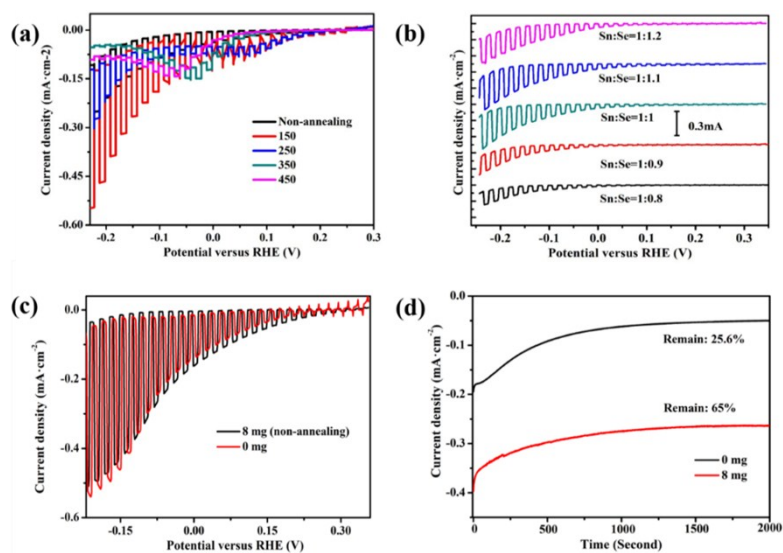


Figure S9. Electrochemical test. (a) Under different thermal annealing sample. (b) Different Sn/Se ratio for 0 mg. These information can screen out the best ratio and annealing thermal for pristine sample. (c) Surface deposited 8 mg selenium on the 0 mg sample. The same J-V curve can prove that the Se element can only repair defects at the annealing process and Se element make no difference of performance. (d)  $J-t$  curve of 0 mg and 8 mg. The higher remain percentage of R-SnSe-M suggests a more stable structure comparing to P-SnSe.

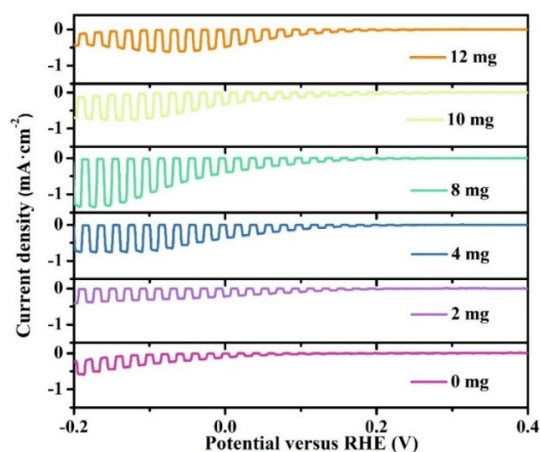


Figure S10.  $J$ - $V$  curve of the SnSe photocathode before and after selenization by different selenium. The photocurrent of the samples increases with the increase of the amounts of Se powders during selenization. When the amounts of Se powders are 8 mg, R-SnSe-M shows an optimal PEC performance with a high limiting photocurrent. Nevertheless, the sample after selenization with Se powders more than 8 mg displays a worse PEC performance than R-SnSe-M.

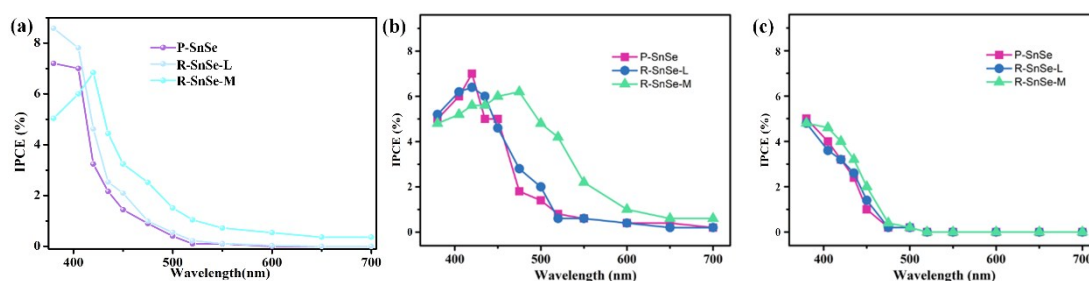


Figure S11. Incident photon-to-current efficiency (IPCE) of P-SnSe, R-SnSe-L and R-SnSe-M in different solutions: (a) 0.05 M  $\text{H}_2\text{SO}_4$  solution at -0.2 V Vs RHE, (b) 0.05 M  $\text{H}_2\text{SO}_4$ -0.05 M  $\text{Na}_2\text{SO}_3$  solution at 0 V Vs RHE, (c) 0.05 M phosphoric acid buffer solution (pH = 6.8) at -0.2 V Vs RHE. In comparison to the other samples, R-SnSe-M shows a higher IPCE due to light absorption red-shift. In addition, when the OER is displaced by sulfite oxidation reaction in 0.05 M  $\text{H}_2\text{SO}_4$ -0.05 M  $\text{Na}_2\text{SO}_3$  solution, R-SnSe-M achieves a light-to-current conversion at least from 650 nm, which is consistent with its band gap.

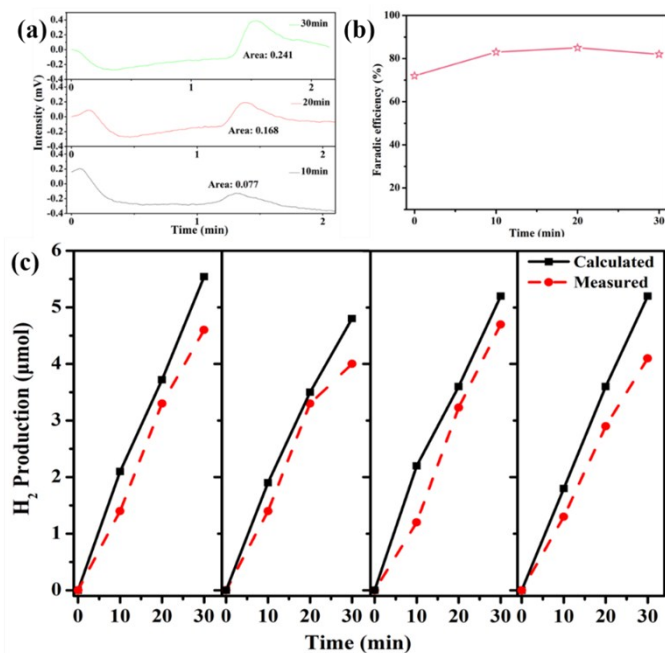


Figure S12. (a) Gas chromatographic data obtained at 10 minutes, 20 minutes, and 30 minutes. (b) Faradaic efficiency was obtained from R-SnSe-M. (c) Photoelectrochemical hydrogen production for the repaired SnSe photoelectrode via calculating and measuring in test conditions. The gas-tight photoelectrochemical cell was applied to collect and measure the increased H<sub>2</sub> production with a volumetric pipette. The volumes of cell and electrolyte were 220 and 70 ml, respectively. The collected gas was further measured by gas chromatography (Lunanruihong Co. Ltd., SP-7820).

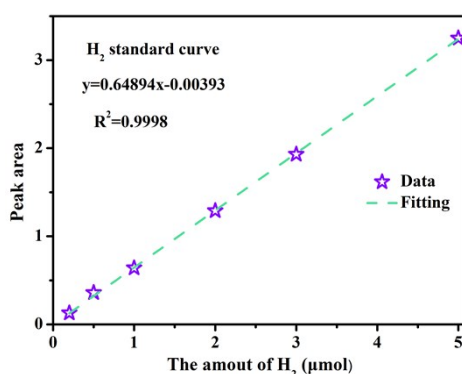


Figure S13. Calibration curve used the determination of hydrogen gas by gas chromatography.

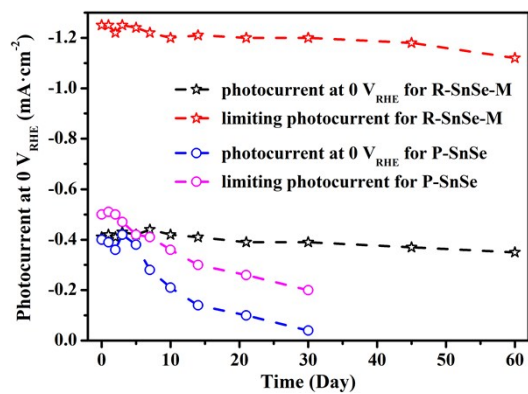


Figure S14. Photoelectrochemical performance of the samples as a function of storage time in the atmosphere.

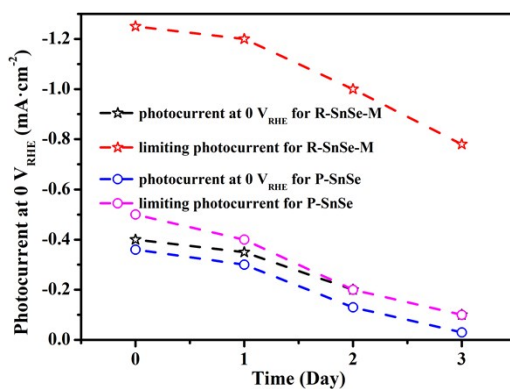


Figure S15. Photoelectrochemical performance of the samples as a function of storage time in 0.05 M H<sub>2</sub>SO<sub>4</sub> solution.

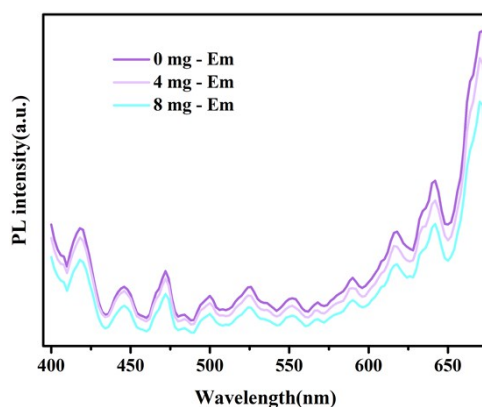


Figure S16. Photoluminescence emission spectra of 0 mg, 4 mg and 8 mg. The lower PL intensity indicates lower photo-charge recombination efficiency.

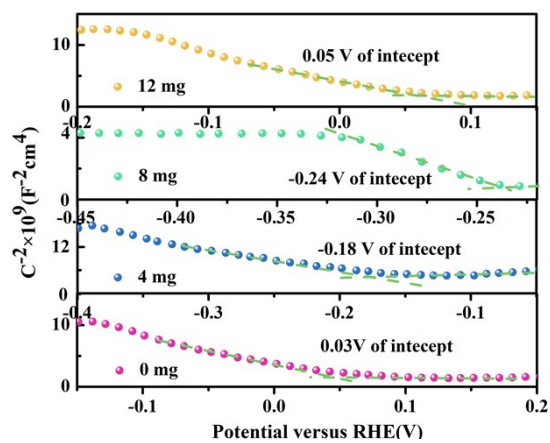


Figure S17. Mott-Schottky plots of 0 mg, 4 mg, 8 mg and 12 mg

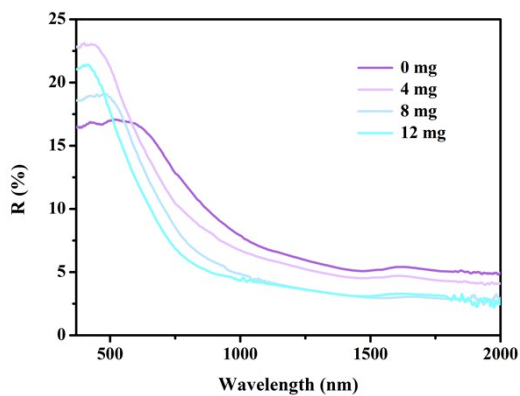


Figure S18. The measured total hemispherical optical reflectance of 0 mg, 4 mg, 8 mg and 12 mg in air.

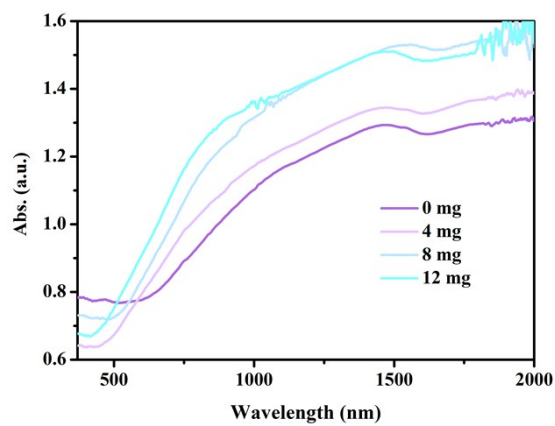


Figure S19. Optical absorb spectra of 0 mg, 4 mg, 8 mg and 12 mg.

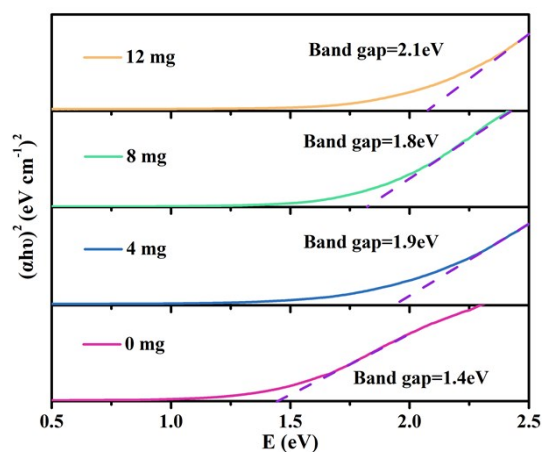


Figure S20. Optical absorption coefficients  $\alpha$  as a function of the incident photo energy  $E$  for direct allowed transition for the 0 mg, 4 mg, 8 mg and 12 mg.

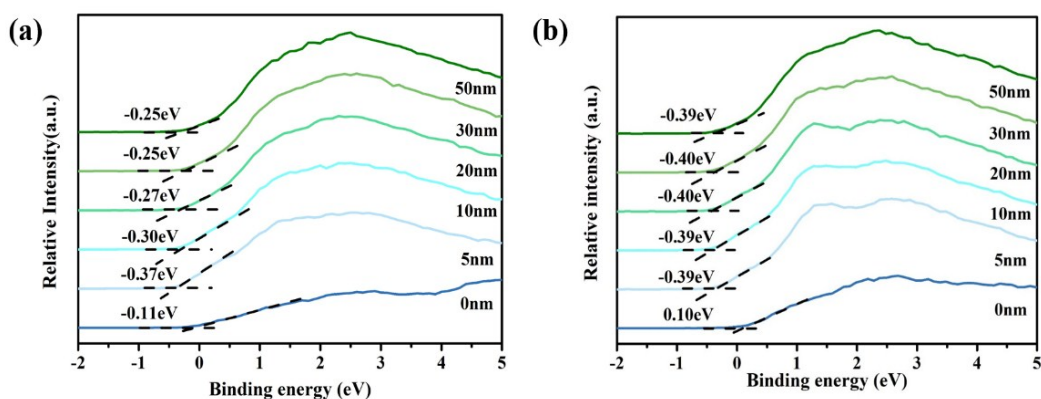


Figure S21. XPS valance band (VB) spectra of (a) 0 mg and (b) 8 mg for each layer.

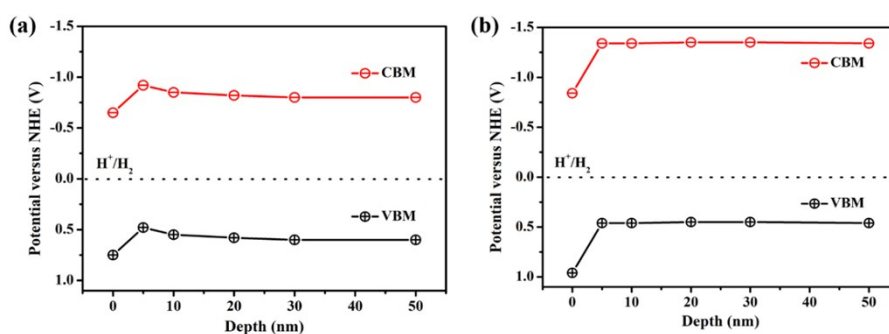


Figure S22. Electron transition simulated pattern for 0 mg and 8 mg. The transition simulated indicates the level of difficulty for electron reacting with  $H^+$  ion (at  $0 V_{RHE} H_2/H^+$ ).

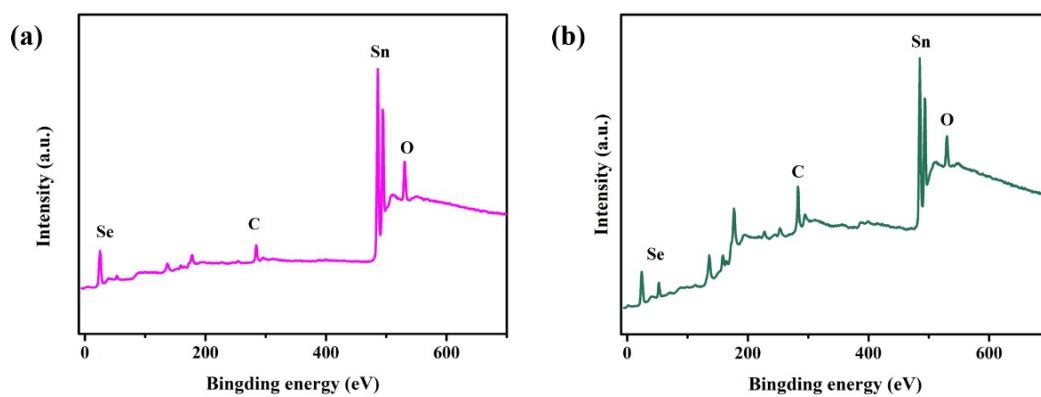


Figure S23. XPS survey spectra of (a) 0 mg and (b) 8 mg

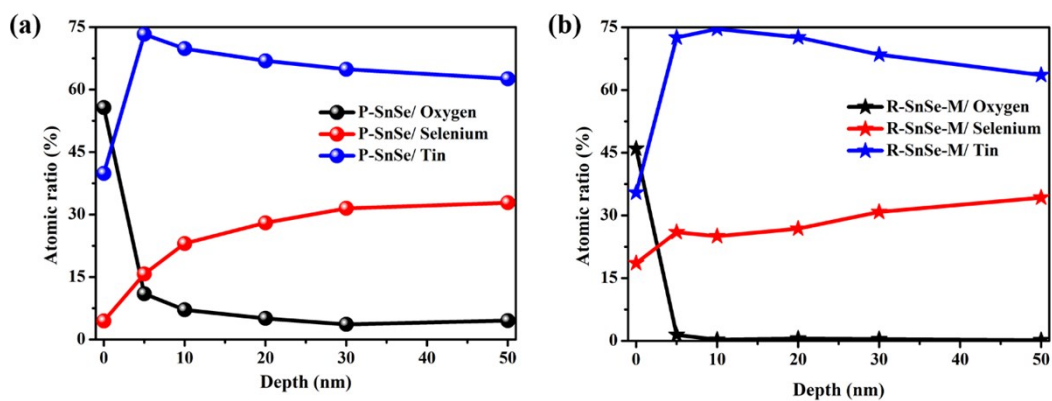


Figure S24. Element depth profile of (a) 0 mg and (b) 8 mg.

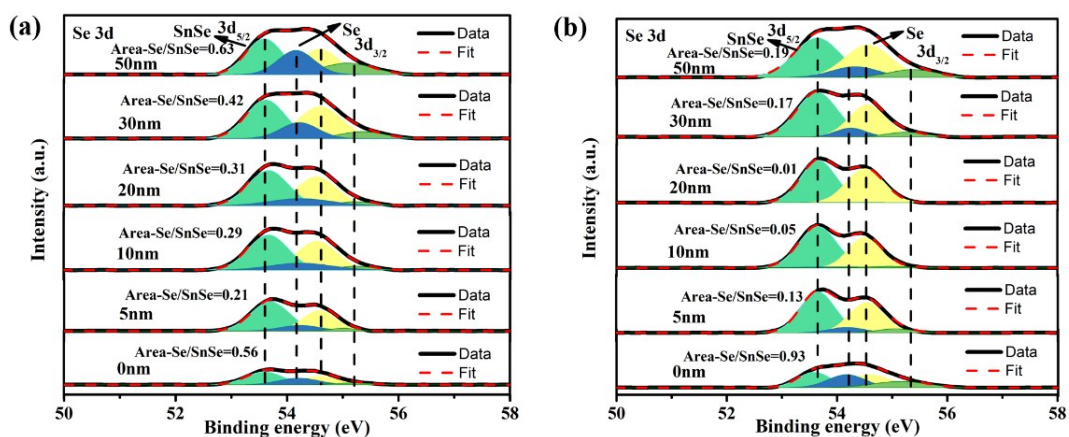


Figure S25. Se 3d XPS Spectra for (a) 0 mg (b) 8 mg

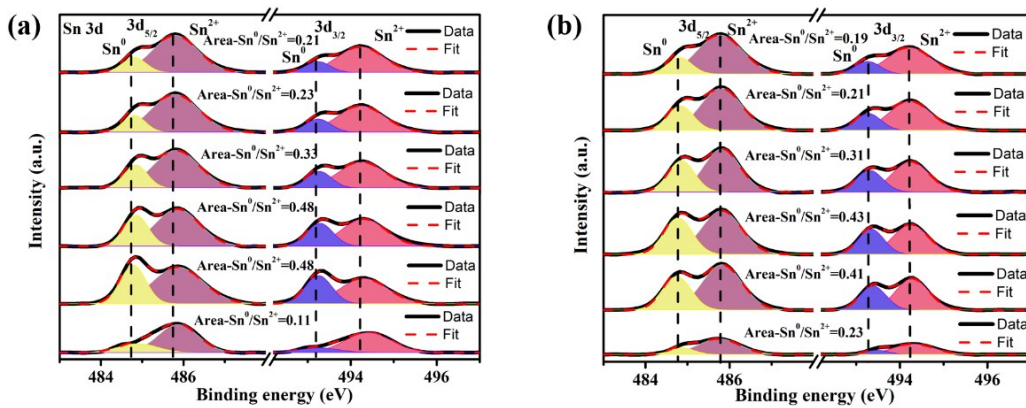


Figure S26. Sn 3d XPS Spectra for (a) 0 mg (b) 8 mg

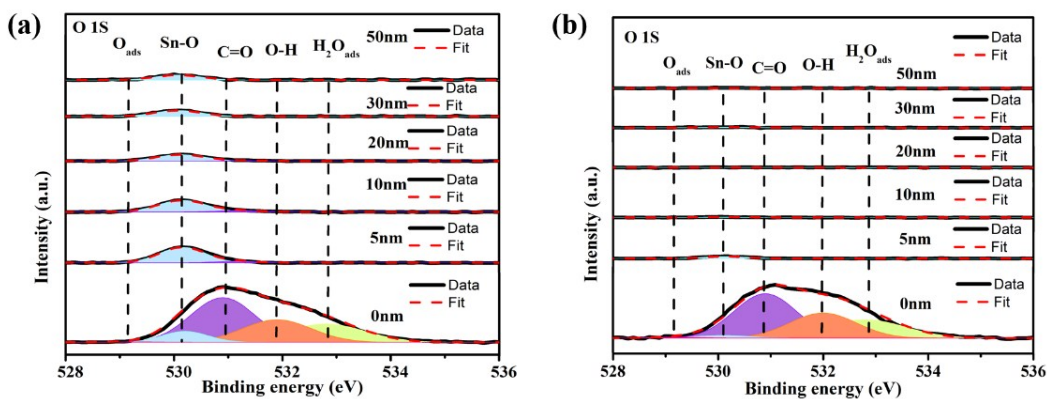


Figure S27. O 1S XPS Spectra for (a) 0 mg (b) 8 mg

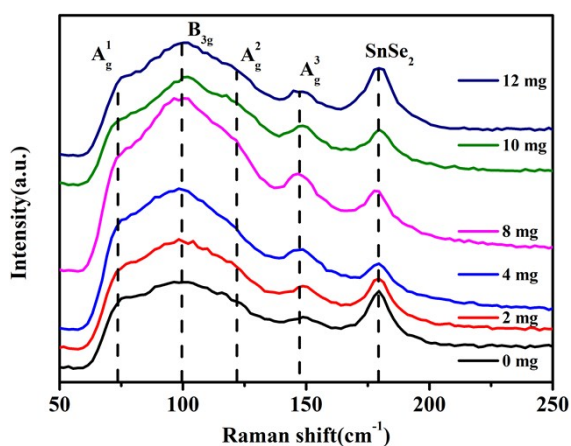


Figure S28. Raman spectra of all sample is shown to an increase or decrease tendency.